ISSN 1990-7931, Russian Journal of Physical Chemistry B, 2016, Vol. 10, No. 2, pp. 245–259. © Pleiades Publishing, Ltd., 2016.
Original Russian Text © S.V. Stovbun, S.N. Nikol'skii, V.P. Mel'nikov, M.G. Mikhaleva, Ya.A. Litvin, A.N. Shchegolikhin, D.V. Zlenko, V.A. Tverdislov, D.S. Gerasimov, A.D. Rogozin, 2016, published in Khimicheskaya Fizika, 2016, Vol. 35, No. 4, pp. 20–35.

KINETICS AND MECHANISM OF CHEMICAL REACTIONS. CATALYSIS

Chemical Physics of Cellulose Nitration

S. V. Stovbun[a, *], S. N. Nikol'skii[a], V. P. Mel'nikov[a], M. G. Mikhaleva[a], Ya. A. Litvin[a], A. N. Shchegolikhin[a], D. V. Zlenko[a], V. A. Tverdislov[a], D. S. Gerasimov[b], and A. D. Rogozin[b]

[a] *Semenov Institute of Chemical Physics, Russian Academy of Sciences, Moscow, Russia*

[b] *Aleksin Chemical Plant, Aleksin, Tula oblast, Russia*

**e-mail: s.stovbun@chph.ras.ru*

Received August 10, 2015

Abstract—The physical mechanisms responsible for the kinetics of nitration of cellulose raw materials of different origin have been studied. It has been shown that the main nitration rate-limiting factor is the speed of untwisting of supercoiled cellulose fibers. This process limits the penetration of nitrating agents into microcrystalline regions and, thus, the total reaction rate. The constructed physical model provides an adequate explanation of all the experimentally observed features of the cellulose nitration process, particularly as a function of cellulose origin (cotton, flax, wood) and preparation/treatment methods (sulfite, sulfate, bleached, refined with sulfurous or boric acids or acetone). The theoretical results have been tested in practice.

Keywords: cellulose, nitration, physical model, structure formation, hierarchical systems

DOI: 10.1134/S199079311602024X

INTRODUCTION

Cellulose, whose annual world production is on the order of 200 million tons, is the most important and popular natural biopolymer. The major users of cellulose are the paper-making and chemical industries, which convert the feedstock mostly to various cellulose esters, such as nitrates or acetates [1]. The most technologically convenient and most commonly used feedstock for chemical production is cotton cellulose.

In the Russian Federation, cotton plant is not grown at all, while commercial cellulose of wood origin is produced from domestic raw materials, particularly for export. At the same time, commercial wood cellulose does not meet the requirements of the *GOST* (State Standard) for esterification; the known esterification processes do not occur efficiently. Thus, commercial softwood cellulose manufactured at the Arkhangelsk and Syassky Pulp and Paper Mills (PPMs) is not nitrated to the level of nitration of cotton cellulose under comparable conditions; this fact has not yet been clearly explained in terms of conventional scientific approaches [1].

Typically, the chemistry of cellulose nitration is studied without taking into account the structural and kinetic characteristics of the reaction. In concentrated acids, the nitration reaction consists in an electrophilic attack of the OH groups of cellulose by the nitronium cation to abstract the proton and form a respective nitrate, or the S_E1 electrophilic substitution reaction. The nitronium ion content in the reaction acidic mixture (RAM) is a few tens percent. Thus, in this study, the used RAM had the following composition: H_2SO_4, 67.4%; HNO_3, 25.4%; and H_2O, 7.2%, which corresponds to a 62.5% conversion of nitric acid to nitronium ions [2]. It is assumed that the nitronium cation rapidly undergoes diffusion in both the amorphous and crystalline regions of the cellulose fiber; therefore, the reactions are formally treated as liquid-phase reactions [1]. At the same time, it is clear that cellulose (both cotton and wood) is a disordered heterogeneous system characterized by a chaos of anisometric structural elements (Fig. 1); the equivalence of it to a homogeneous reaction system is not obvious.

A fairly large number of studies have addressed the kinetics of cellulose nitration. The kinetics of nitration of wood cellulose in a mixture of nitric acid and dichloroethane has a pronounced two-stage pattern [3]. The first reaction stage is more rapid; it occurs about 100 times faster and takes only a few minutes; it yields a nitrocellulose (NC) with a degree of substitution of about 2.0–2.2. In the slower stage, which takes a few tens of minutes, the degree of substitution achieves a value of ~2.5 [3]. Under quasi-homogeneous conditions, nitration of cotton cellulose with aqueous solutions of nitric acid occurs much more rapidly; it takes about a minute or less and yields a nearly pure cellulose trinitrate [4]. The observed differences are evident from the dependence of the degree of heterogeneity of the final NC on the real concentration of the nitrating agent (nitronium ion) in

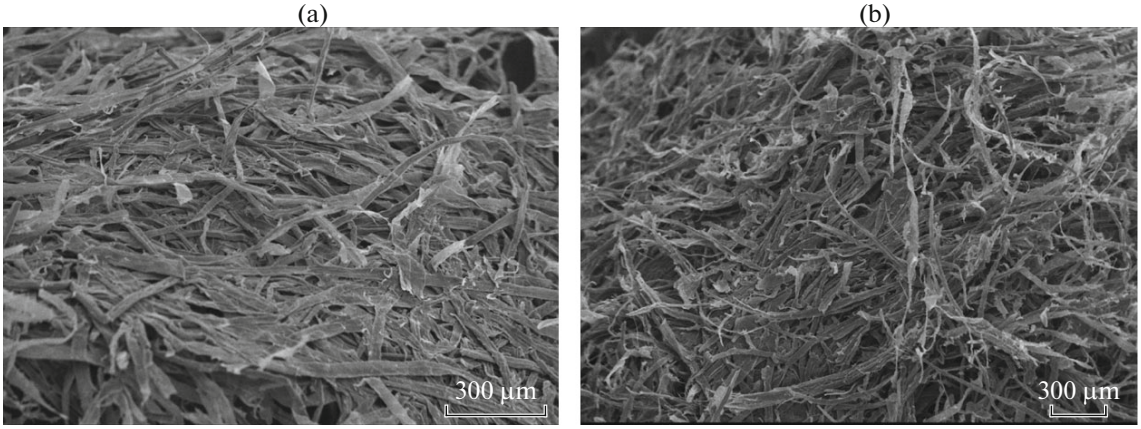

Fig. 1. Electron micrograph (Phenom G2 Pro) showing the chaos of the structural elements of semibleached sulfite wood cellulose: (a) without treatment and (b) after nitration.

the reaction mixture [5, 6]. The higher the concentration, the more heterogeneous the final product; this relationship is attributed to the specific features of diffusion of active nitronium ions in the cellulose matrix [5] and agrees well with the scheme represented in this study. It was found that the activation energy of nitration of cotton cellulose with vapors of nitric acid [7] and nitrogen dioxide [8] is about 40 kJ/mol of nitro groups. In addition, for this system, it was shown that the effective diffusion coefficient of the nitrating agent in the cellulose matrix is ~10^{-7} cm^2/s [7, 8].

Previously, the physicochemical processes in cellulose were described using the averaging scales that made it possible to reduce a heterogeneous problem to a phenomenological homogeneous model. Thus, according to the approaches discussed in the 1970s and 1980s, the kinetics of diffusion-controlled reactions in wood can be described using the concepts of formal isokinetic zones [9, 10]. Isokinetic zones have different characteristic reaction times, which differ by orders of magnitude; as a consequence, the total kinetic dependence has a logarithmic form (polychronic kinetics) [11]. It is now becoming clear that phenomenological approaches have not revealed the structural features of chemical processes of wood cellulose esterification and have not led to a significant technological progress.

However, there is every reason to believe that, even under conditions of a high hydromodulus (~50) in cellulose processing, all the major physicochemical processes take place inside an isolated fiber which mostly preserves its morphology and has a well-known structural organization (Fig. 2) characterized by the presence of supercoiling and hierarchical chiral phases [12]. Cellulose is known to comprise compact crystalline regions—elementary fibrils—composed of complementarily packed helical macromolecules, which in turn are helically twisted to form microfibrils. Moreover, the structural chiral hierarchy of cellulose obeys the general laws governing the structure formation that

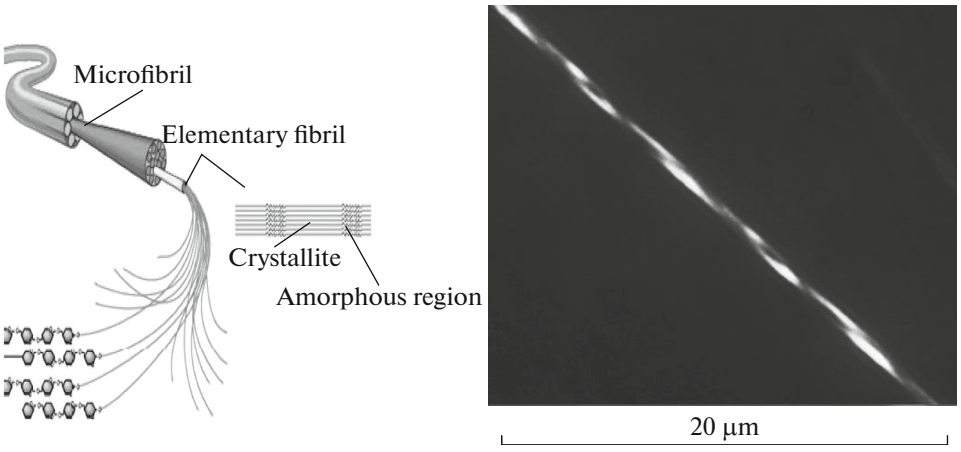

Fig. 2. Structure of the cellulose fiber. Comparison of the hierarchical structure of the fiber with a supramolecular TFAAS string.

Table 1. Content of α-cellulose in commercial cellulose samples

Sample designation*, manufacturer	ω, %
RB, OAO Arkhangelsk PPM	85.3
UZ Cell	94.1
SKhP, OAO Syassky PPM	81.6
CKhZh, OAO Syassky PPM	81.6
ALP, OAO Arkhangelsk PPM	81.8
VLV, Vologda	85.2
ALZh, OAO Arkhangelsk PPM	81.0
AKhZh, OAO Arkhangelsk PPM	82.5

*A more detailed description of the cellulose types is provided in the text.

were previously determined for chiral biomimetic systems [12, 13].

It has been first shown by the authors elsewhere that the formation of hierarchical chiral phases and supercoiling are a fundamental principle of structure formation in chiral biomimetic and living systems [13]. At the same time, it is quite obvious that it is the macroscopic dynamics of winding–untwisting in the supercoiling of fibrils and macromolecules [14] that can limit the access of reactants to the compact phases of cellulose fibers. In this respect, an adequate physical model of a cellulose fiber is a hierarchical supercoiled supramolecular string in which helical structures are observed on a scale of 2 nm to 10 μm. These scales correspond to the scales of helical structures formed by trifluoroacetylated amino alcohol (TFAAS) biomimetics, the macroscopic dynamics of which and the features of formation of compact phases were previously studied by the authors [14, 15].

The aim of this study was to construct a physical model of the nitration process that, taking into account the characteristics of structure formation in chiral systems, would make it possible to explain the specific features of nitration of wood, flax, and cotton cellulose and prepare samples with a high nitrogen content. To this end, the following was studied: (i) the morphology of cellulose and NC; (ii) the kinetics of exothermic nitration reactions; and (iii) the circular dichroism (CD) of nanocellulose (NNC) gels, the macroscopic dynamics of untwisting of cellulose fibrils, and their van der Waals interactions.

MATERIALS AND EXPERIMENTAL METHODS

The following types of cellulose were used:

—Viscose sulfite cellulose (roll paper), OAO Arkhangelsk PPM (RB).

—Cotton Cellulose, UZ Cell.

—Semibleached softwood sulfite cellulose (folder), OAO Syassky PPM (SKhP).

—Bleached softwood sulfite cellulose (liquid flow), OAO Syassky PPM (SKhZh).

—Bleached sulfate cellulose LS (folder), OAO Arkhangelsk PPM (ALP).

—Flax cellulose VLV (Vologda).

—Bleached hardwood sulfate cellulose (liquid flow), OAO Arkhangelsk PPM (ALZh).

—Bleached softwood sulfate cellulose (liquid flow), OAO Arkhangelsk PPM (AKhZh).

—A gel prepared in the form of a nonsedimenting suspension of NNC in water using a colloid mill. The samples were prepared by mixing an aqueous solution of $NaHSO_3$ or H_3BO_3 with NNC in a volume ratio 1 : 1 and subsequent gentle shaking of the resulting mixture. The weight concentrations (%) of $NaHSO_3$ are given below for the aqueous solution before mixing with NNC; that is, the $NaHSO_3$ concentration in the mixture is 2 times lower.

The alpha-cellulose content in the commercial celluloses produced at the PPMs is 81–85%. Since only bleached brands of softwood and hardwood celluloses are regarded as original commercial cellulose, the lignin content in them is at a level of a few tens of a percent and meets the requirements of *GOST 595-79*. Furthermore, cold refining leads to an additional decrease in the content of lignins oxidized during bleaching owing to their dissolution in an alkaline solution.

An increase in the α-cellulose content to a level corresponding to *GOST* for cellulose for chemical processing, i.e., to a value of >95%, was achieved via refining the commercial cellulose. Cold refining was conducted in accordance with the procedure specified in *GOST 6840-78* for the determination of α-cellulose content in commercial celluloses by the weight method. The process included the following steps: (i) treatment of an air-dry commercial cellulose with an aqueous sodium hydroxide solution with a concentration of 17.5% (hydromodulus of 15) for 45 min; (ii) dilution of the resulting mass to an alkali concentration of 9.5%; (iii) vacuum filtration and rinsing with three portions of a 9.5% alkali solution (total volume corresponds to a hydromodulus of 25); and (iv) washing with water to neutral pH. It was shown that cold refining of original cellulose in the form of a wet mass for 10–30 min leads to the formation of cellulose with a 98% content of α-cellulose. The measurement results are shown in Table 1.

Test experiments were aimed at determining the basic parameter of NC—nitrogen content—and studying the kinetics of nitration and obtaining additional data on the processes that occur during nitration. The nitrogen content in NC was determined by several methods—elemental analysis, titrimetry, and gravimetry—that were developed in the course of the study.

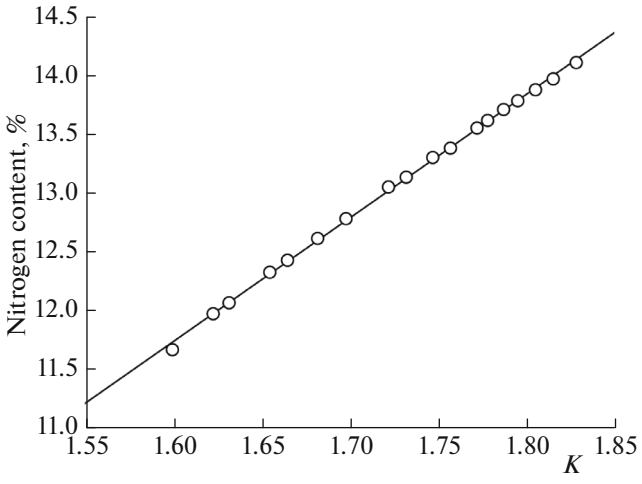

Fig. 3. Percentage of nitrogen in the NC versus cellulose weight change ratio during nitration.

Elemental analysis was conducted using a CE1106 automated CHN analyzer (Italy). The weighed portion of the sample was 0.8–1 mg. The burning temperature of the sample was 1050°C. The flash point in oxygen for the sample in a tin capsule was 1800°C. Oxygen was dosed using a loop-shaped edosing device. Separation of degradation products (nitrogen, carbon dioxide, and water) was provided by gas chromatography. The CHN content was calculated automatically by the software of the instrument. The program took into account calibration coefficients determined from reference standards, blank experiment results, and the weighed portion magnitude. The absolute error of the method was 0.30–0.50%. The complete analysis cycle time was 10 min.

SOP 2014-03 technique of OOO Biovet-ferment. The titrimetric method for the determination of the weight fraction of nitrate nitrogen consists in the decomposition of a weighed portion of the test sample with hydrogen peroxide and the reduction of the nitrate nitrogen to ammonia with a Devarda's alloy in the presence of sodium hydroxide. The amount of ammonia is determined by back titration of excess sulfuric acid after the absorption of ammonia. The analysis duration is 4 h.

Rapid gravimetric method for the determination of the degree of nitration of cellulose (Semenov Institute of Chemical Physics, Russian Academy of Sciences). The nitration of cellulose consists in the substitution of the hydrogen atom of the hydroxyl groups of cellulose by NO_2; it is accompanied by a significant change in the weight of the elementary unit of the cellulose. This feature makes it possible to calculate the dependence of the sample weight change during nitration on the degree of substitution of hydroxyl groups by nitro groups. During nitration, the $C_6H_{10}O_5$ cellulose elementary unit transits into the $C_6H_{10-3x}N_{3x}O_{5+6x}$ elementary unit, where $0 < x < 1$ is the degree of substitution of H by NO_2, i.e., the ratio between the average number of substituted hydroxyls and their total number equal to 3.

Figure 3 shows the plot of the dependence of nitrogen content (wt %) on the weight change ratio (K), i.e., the weight ratio between NC and original cellulose. It is evident from the figure that the weight fraction of nitrogen in the NC, to a high precision, linearly depends on the weight change ratio during nitration: $\omega = 0.1057K - 0.0517$.

The rapid gravimetric method is based on the assumption that the substitution of hydroxyl groups by nitro groups is the only process that occurs during nitration. It is assumed that a possible contribution of the formation of acid sulfo esters $-COSO_2H$ is negligible. This assumption has been confirmed by elemental analysis, which has not revealed the presence of sulfur in the samples. The results of determination of the nitrogen content by the gravimetric and elemental analysis methods are almost the same.

In the experiments, air-dry cellulose strips with a weight of about 50 mg, which were preweighed on an analytical balance with a precision of up to ±0.1 mg, were immersed in a nitrating mixture (RAM) placed in a sealed glass container at a predetermined temperature; after certain time intervals, the strips were withdrawn. After that, the sample was immersed in a 60% sulfuric acid solution. The acid of this concentration was used as a water-containing medium to provide the instantaneous cessation of nitration and the intermediate dilution of concentrated sulfuric acid before immersing the sample into ice water to avoid strong heating during the dilution of sulfuric acid with water. The sample was exposed to 60% sulfuric acid for 30 s and then rapidly transferred into ice water. Next, the sample was immersed into distilled water (100 mL) for 10–15 min and then into a sodium bicarbonate solution for 30–40 min. After that, the sample was washed with water 3 or 4 times with holding in a large volume (~100 mL) for 10–15 min. Next, the wet samples were pressed between two sheets of filter paper and finally dried on the paper at room temperature. Final drying was conducted in a drying cabinet at a temperature 60°C. The degree of substitution was determined using the well-known formula [1]

$$\alpha = \frac{3.6N}{31.1 - N}. \quad (1)$$

Optical microscopy was conducted using the following instruments:

—a Mikmed-6 optical microscope (LOMO, Russia);

—a Carl Zeiss Jena optical microscope (Germany);

—a Nikon optical digital microscope (Japan);

—a computerized optical bench (Research system microscope) based on an Olympus BX51 microscope (Japan);

—a Veeco VCM-200 confocal optical microscope;

—a Leica DMI 6000 inverted optical microscope.

Electron microscopy was conducted using the following equipment:

—A Phenom G2 pro scanning electron microscope, which allows imaging in a magnification range of 80× to 45 000× at a resolution of up to 25 nm.

—A Hitachi700 transmission electron microscope.

Atomic force microscopy. All measurements by scanning probe microscopy were conducted on a Solver HV atomic force microscope (AFM; ZAO NT-MDT, Zelenograd, Russia) operating in the tapping mode at room temperature and atmospheric pressure. A cellulose sample was placed on the surface of a standard silicon wafer used in the microelectronics industry, and the wafer with the sample was fixed in the AFM.

AFM measurements of the surface topography of the sample were conducted with a gradual scaling-up of the frame in a range of 10 000 to 4 μm^2. Standard cantilevers manufactured at ZAO NT-MDT (Zelenograd, Russia) were used. The natural frequencies of the cantilevers were in a range of 110–180 kHz; the tip curvature radius was 10 nm. Most of the data were obtained in the constant amplitude mode; the rest, in the phase contrast distribution mode. In the topographic images recorded in the constant amplitude mode, the height is represented by means of color: the higher the location of the topography element, the lighter the color.

Dynamic viscosity of refined cellulose. The most important characteristic of cellulose intended for chemical processing is the average degree of polymerization of the cellulose macromolecules, which is estimated from the dynamic viscosity of cellulose solutions according to *GOST 14363.2*. Table 2 shows the results of measurement of the dynamic viscosity of various cellulose types after cold refining (α index). These data suggest that the viscosity values depend on the nature of the feedstock and vary in a range of 35–96 cP, which meets the requirements of *GOST*. The lowest viscosity is exhibited by softwood cellulose; the highest viscosity is found in celluloses based on a hardwood mixture. Flax cellulose occupies an intermediate position. The above results suggest that, for these types of feedstock, the step of controlling the degree of polymerization can be omitted.

CD coefficients were measured using an SKD-2 CD spectra analyzer, which provides the operating temperature stabilization in a range of 25–75°C, at wavelengths of 250–750 nm. A 2-mL solution was pipetted into the cuvette of the analyzer. The cuvette was placed in the working cell of the basic unit of the analyzer. Measurements were conducted at a relative humidity of 50–55%.

Raman spectra of the solid products were recorded using a RamanStation-400 Raman spectrometer (PerkinElmer). This instrument is equipped with a diode laser with λ_{ex} = 785 nm (100 mW) for the excitation of Raman scattering, an iDus-420 detector (Andor) thermoelectrically cooled to –60°C (1024 × 255 pixel Si-CCD matrix) for Raman spectrum recording, and a motorized *XYZ*-positioning stage and a color video camera with a 30× lens for the visual inspection and selection of the sample portion for analysis (a spot with a diameter of about 5–10 μm) or laser-beam focusing on the test sample before recording the Raman spectrum. During spectra recording, the video camera lens is used for transmitting a focused laser excitation onto the sample and, at the same time, for collecting the sample-generated Raman photons and delivering them to the spectrograph. Owing to the echelle optical design, the instrument contains no moving parts, requires no premeasurement calibration, records the total spectrum in a single scan, and provides a constant optical resolution (1, 1.5, 2, 4, 8, or 16 cm^{-1}) in the entire measured range of Raman shifts (95–3400 cm^{-1}). Raman spectra of cellulose samples (powdered materials mostly of white color) were recorded using samples with a weight of 5–10 mg placed in 50-μL aluminum cups. To increase the sample density and improve the Raman signal, the powder was manually premolded in an aluminum container using a flat-faced metal rod with a suitable diameter. The spectra were recorded at a resolution of 1 or 2 cm^{-1} in a Raman shift range of 100–3200 cm^{-1} at a laser excitation power of 5–75 mW in different experiments with averaging of 9–16 scans at a CCD-detector exposure time of 5–30 s. The instrument management, the selection of experimental parameters, and the spectra processing were conducted using the Spectrum v.10.6 software package (PerkinElmer).

X-ray analysis of the cellulose samples was conducted using a retrofitted DRON-3 X-ray diffractometer with a copper anticathode at a voltage of 30 kV and

Table 2. Dynamic viscosity of the cellulose samples according to *GOST 14363.2*

Sample designation	Dynamic viscosity, cP
SZhP (α) after dispersion on an IKA MagicLab	48
SZhP (α)	49
AKhZh (α)	37
AKhZh (α), 1% $NaHSO_3$ solution, 68°C, 60 min	35
AKhZh (α) 0.1 M H_3BO_3, 65°C, 80 min	37
ALP (α)	96
ALP (α) after grinding	92
ALZh (α)	81
VLV (α)	70

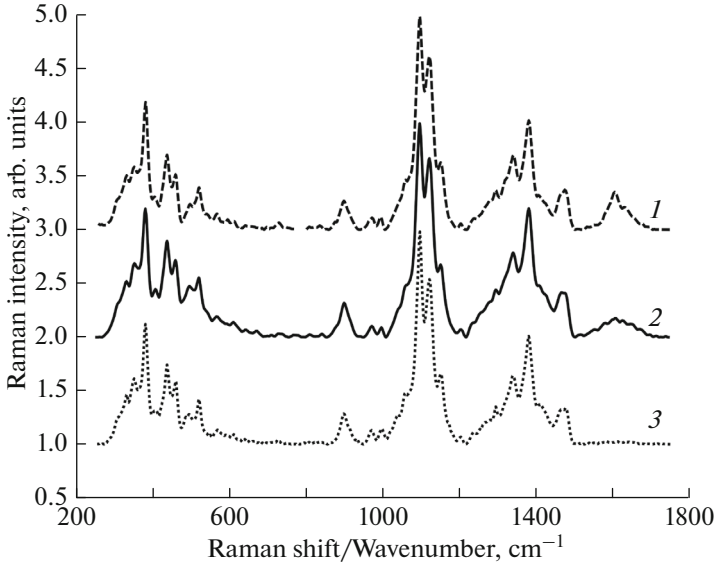

Fig. 4. Raman spectra of original commercial celluloses: (*1*) folder and (*2*) liquid flow of the Syassky PPM and (*3*) bleached cellulose of the Arkhangelsk PPM, roll paper.

a current strength of 20 mA (Ni filter). The X-ray wavelength was $\lambda \approx 0.15$ nm. Measurements were conducted at a temperature of 25°C and a relative humidity of 50–55%. The original sample was placed in a flat glass cell with a diameter of 10 mm and a depth of 1 mm. In some cases, the sample was held in the air or in a vacuum for a certain time.

Preparation of fibrous NNC semiproducts (wood cellulose, cotton cellulose) was conducted using the following IKA dispersing units (Germany): a EuroStar 2000 unit (stirrer with a dissolving nozzle; a rotation speed of 150–450 rpm) and an IKA MagicLab dispersing unit (rotor–stator couple of the colloid mill type; a rotation speed of 10000–18000 rpm). The mass concentration during dispersion was 1–3%.

The process time and the rotor–stator gap in the colloid mill were varied depending on the fibrous semiproduct type. One-percent nonsedimenting nanogels of these NNC semiproducts of wood cellulose causing the Tyndall effect were used.

RESULTS AND DISCUSSION

The elementary structural unit of native cellulose is an unbranched polymer chain of β-D-glucopyranose residues which is bound to other chains, on average, via one or two hydrogen bonds per unit. The macromolecule length can significantly vary. Thus, the degree of polymerization is 2500–3100 for wood cellulose, 9300–10800 for cotton fibers, and 36000 for flax fibers [16, 17]. Native cellulose is composed of two—crystalline and amorphous—fractions [1]. The microcrystalline regions are associated with the elementary cellulose fibrils; the amorphous regions are associated with the low-molecular-weight cellulose fractions located between them [18, 19]. The minimum apparent thickness of the elementary cellulose fibrils is 3–5 nm; it is characteristic of wood cellulose [18]. The thickness of the elementary fibrils of the flax and cotton celluloses is higher; it is 5–6 and 7–9 nm, respectively [20].

The elementary fibrils of softwood cellulose, which are composed of 24 densely and complementary packed macromolecules, have a helical crystalline structure [21]. The packing of macromolecules in elementary fibrils is attributed to the specific features of their biosynthesis; that is, the crystallization and formation of fibrils occur simultaneously during the synthesis thereof [22]. Thus, all celluloses isolated from a particular plant are characterized by a certain cross-sectional dimension of microcrystalline regions.

It is well known that wood cellulose preserves the morphology of the original plant raw material during the industrial separation of it from lignin and hemicelluloses (pulp cooking) [1]. After delignification of wood cellulose, for example, at the Arkhangelsk PPM, individual cellulose fibers are clearly visible in the resulting mass (Fig. 1). Note that the morphology of the prepared cellulose samples does not depend on the isolation method; that is, sulfate or sulfite celluloses of wood origin exhibit an identical morphology. The morphology of the cellulose is preserved even under severe conditions of the nitration reaction (Fig. 1).

An extremely convenient method for studying the morphology and molecular structure of cellulose is Raman spectroscopy (Fig. 4) [1]. It is noteworthy that the original wood celluloses from the different suppliers are very similar in molecular structure, as evidenced by the coincidence of Raman spectra in a

range of 1500–800 cm^{-1} (Fig. 4). Moreover, the original samples exhibit almost the same packing, as evidenced by the identity of the phonon bands at low Raman shifts in a region of 250–600 cm^{-1}, which are responsible for the packing of cellulose macromolecules in the crystalline regions. The differences in the Raman spectra observed in a region of 1700–1500 cm^{-1} are attributed to different lignin content (Fig. 4). The intensity of the Raman band with a maximum in the vicinity of 1600 cm^{-1} decreases in proportion to the degree of bleaching of cellulose, which corresponds to the decrease in the lignin content.

The preservation of the hierarchy of linear scales of native cellulose during delignification and nitration indicates the occurrence of effective structure formation and self-organization of the cellulose macromolecules [1], which severely limit their self-diffusion and subsequent swelling/dissolution of the fibers [1]. This self-organization is caused by supercoiling [12] and the presence of a hierarchy of molecular and supramolecular helical levels—such that the fibers can be represented like a twisted rope—in the cellulose structure. In addition, in wood cellulose, the additional binding of fibrils into fibers via hemicelluloses occurs to a greater extent than in flax or cotton celluloses, which contain significantly lower amounts of low-molecular-weight binding components (hemicelluloses and residual lignin).

Figure 5 shows the experimental kinetic curve of nitration of softwood cellulose produced at the Arkhangelsk PPM (AKhZh) after refining it with a NaOH solution, i.e., after removal of low-molecular-weight hemi-, β-, and γ-celluloses playing the role of a component that binds the supercoiled fibrils. In the case of nitration of the refined cellulose, the nitrogen content achieves 13.5%; however, under the same nitration conditions for the original cellulose, it does not exceed 12%. The kinetic curve of nitration exhibits two pronounced stages [3], namely, a fast stage, in which the nitrogen content achieves ~12.5% within 2–3 min, and a slow stage, in which an additional nitrogen amount of 0.5–1.0% is "gained" within 25–30 min (see Fig. 5).

The expansion of the kinetics of nitration in two exponents gives characteristic times of ~0.5 and ~10 min (Fig. 5). In view of the above described features of the hierarchical structure of cellulose, it apparently can have only two compact organization levels. Therefore, only two effective isokinetic zones should be considered; one of the zones is the region inside the elementary fibrils with diameter X of less than ~10 nm; the other zone is the region inside the microfibrils with a diameter of less than ~100 nm, which seems to be consistent with the behavior of the observed two-exponential kinetics.

Based on the concept of the two isokinetic zones, the time of molecular diffusion during cellulose nitration for $D \sim 10^{-11}$ m^2/s is determined as follows [23]:

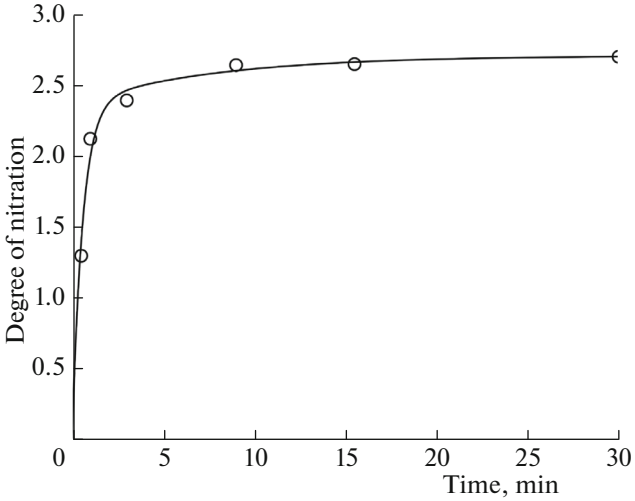

Fig. 5. Kinetic curve of nitration of softwood cellulose in the form of a loose folder ($\rho \sim 0.2$ g/cm^3) with a thickness of about 1 mm at 20°C. The circles and the line show the experimental data and the two-exponential approximation, respectively, with characteristic times of 36 s and 7.6 min, respectively.

$$\tau = \frac{\langle X^2 \rangle}{6D} = 0.4\left(10^{-6} - 10^{-4}\right)\text{s}. \qquad (2)$$

However, comparison of the found diffusion time with the characteristic times of nitration to degrees of substitution of 1–2 suggests that nitration is not limited to molecular diffusion. The estimation of the diffusion coefficient from characteristic times of the slow nitration stage also leads to diffusion coefficient values of $D \sim 10^{-18}$–10^{-20} m^2/s, which do not have any physical sense for low-molecular-weight compounds [23]. Thus, the estimates show that molecular diffusion is not the rate-limiting step of nitration at any conversion value.

Since in the conventional scheme of nitration it is the nitronium ion that acts as a reaction agent [24], it is necessary to explore the possibility of transfer of charged particles inside microcrystalline cellulose regions at high degrees of nitration. The surface of nanofibrils is much more highly accessible to nitrating agents than their internal volume; therefore, it is the surface that is first nitrated. Based on the data that a cotton cellulose nanofibril consists of 24 cellulose chains [21], it is easy to calculate that the fraction of OH groups located on the elementary fibril surface is 1–1.4 per residue. This result is in good agreement with the experimentally observed threshold of the beginning of structural rearrangements of the cellulose matrix during nitration. It is the degree of substitution of ~1.3 that provides the occurrence of reflections corresponding to crystalline cellulose trinitrate in the X-ray diffraction patterns (Fig. 6).

The cellulose nitration experiments revealed a significant threshold variation (1.3-fold) in the free vol-

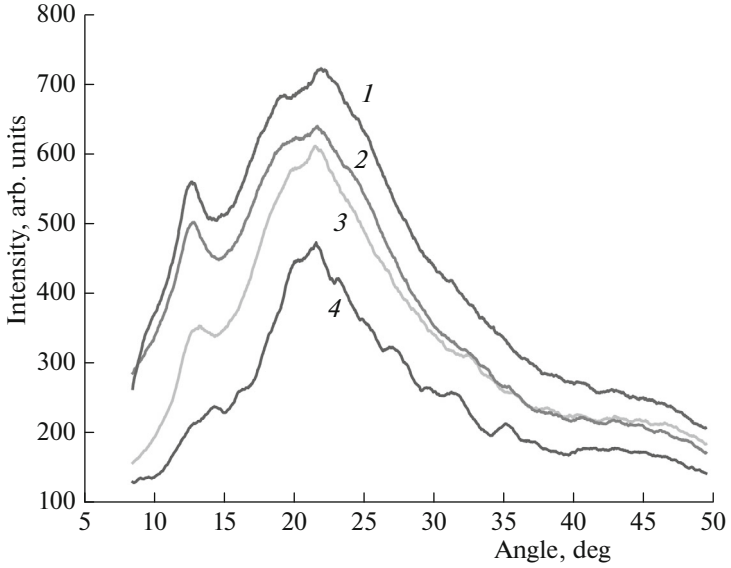

Fig. 6. Variation in the X-ray diffraction patterns of cellulose during nitration for degrees of substitution of (*1*) 2.64, (*2*) 2.40, (*3*) 2.12, and (*4*) 1.3. The peak in the region of 12°–15° corresponds to crystalline cellulose trinitrate.

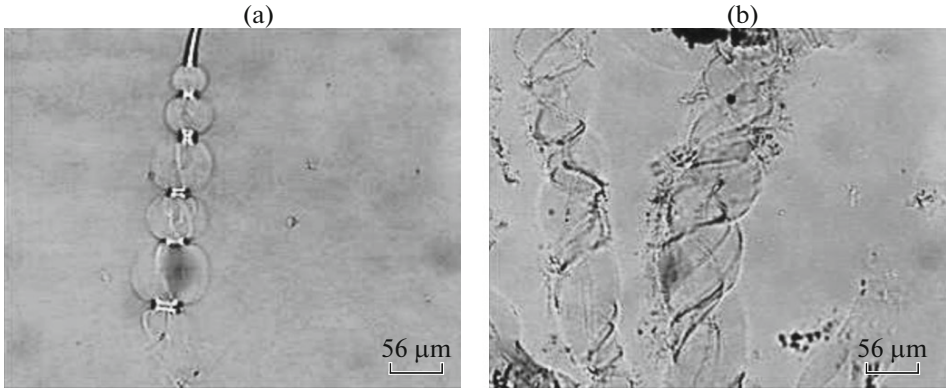

Fig. 7. Untwisting of spruce tracheids in concentrated sulfuric acid. Published by courtesy of E.V. Novozhilov [27].

ume of the fiber or swelling thereof (Fig. 7) at a degree of substitution of 1.1–1.3, i.e., at the values providing a change in the X-ray diffraction patterns. It is obvious that the surface layer of the elementary fibril is the first to undergo nitration.

As cellulose nitrate accumulates in the surface layer of microfibrils, their internal volume is surrounded by a layer of hydrophobic densely packed NC [5], which prevents the penetration of nitronium cation inside the fibrils. In fact, the Born energy of transfer of a monovalent ion with a radius of $r \sim 1.5$ Å [25] from a medium with a dielectric constant of about $\varepsilon_2 \sim 100$ into a hydrophobic region ($\varepsilon_1 \sim 1$–5) is, on the average, as follows [26]:

$$\Delta G = -\frac{q^2}{8\pi\varepsilon_0}\left(\frac{1}{\varepsilon_1}-\frac{1}{\varepsilon_2}\right) \sim 1\text{–}1.5 \text{ eV}. \qquad (3)$$

At this activation energy, the penetration of NO_2^+ inside a fibril takes a time longer than 3×10^4 s, which should actually stop the nitration process. This effect is fundamental for an increase in the heterogeneity of the final NC with increasing actual nitronium ion concentration in the reaction mixture [5, 6].

Thus, nitration is undoubtedly associated with the structural rearrangement of elementary fibrils, during which macromolecule fragments become accessible to interaction with nitronium ions. In addition, the structural rearrangement of fibrils is dynamic and reversible because the morphology of the original and nitrated celluloses is almost the same (Fig. 1).

The previously observed effects of reversible swelling of cellulose fibers in various solvents [1] lead to the formation of microscopically observed blisters, i.e., bulbs, which in fact are regions of an unwound fibril of

an increased volume. The formation of these bulbs during the swelling of a cellulose fiber in sulfuric acid is shown in Fig. 7 [27].

According to Euler [28], during the twisting of strands, the friction forces exponentially depend on the number of turns:

$$F \sim \exp(2\pi\alpha n), \quad (4)$$

where n is the number of turns and α is the coefficient of friction. Therefore, the swelling of a cellulose fiber without untwisting thereof is unrealistic.

In other words, the supercoiled structure of the fiber and the macroscopic dynamics of untwisting of supercoiled hierarchical structures [11] are factors that determine the kinetics of chemical transformations during nitration. Note that, taking into account the above Euler's energy restriction (4), the observed swelling and bulb formation processes (Figs. 7, 8) are, in fact, experimental evidences of the reality of untwisting of cellulose fibers.

Consider the kinetics of nitration of the refined (purified from low-molecular-weight impurities) wood cellulose at varying temperatures (Fig. 9). At positive temperatures, the initial portion of the kinetic curve of nitration has a pronounced linear pattern (Fig. 9). Moreover, at a temperature of −10°C, the kinetics is linear over the entire range of observation. This form of initial portions corresponding to a zero-order reaction takes place if the reaction rate depends on the OH group concentration only slightly or does not depend at all. Formally, this situation is implemented if the dimensions and characteristics of the region in which the reaction occurs do not change with time. The occurrence and stability of parameters of this region can be attributed to effective nitration only in the region of untwisting of elementary microfibrils. In this case, at a constant untwisting speed, the reaction will occur only in a cylindrical volume with length l comparable, for example, with the size of a bulb in an untwisting fiber or fibril (Fig. 8). Therefore, the reaction rate will be a constant and the total kinetics will be of zero order.

Substitution of the experimental data shows that a change in the nitration rate constant with increasing temperature in the initial portion is satisfactorily described by the Arrhenius equation with an activation energy of $E_a \approx 46$ kJ/mol and a preexponential factor of $K_0 \approx 4.5 \times 10^5\ s^{-1}$. The respective rate constants were estimated from the slopes of the kinetic curves in Fig. 9. In this case, total time τ_{tot} of two successive processes—the formation of a reaction site for time τ_c and the collision of the nitronium ion with the OH group for time τ_{coll} is $\tau_{tot} = \tau_{site} + \tau_{coll}$, while the frequency is $\nu_{tot} = \nu_{site}\nu_{coll}/\nu_{site} + \nu_{coll}$. Since the frequency of collisions of the nitronium ion with the OH group has a value of $\sim 10^{12}\ s^{-1}$ and the relationship $\nu_{coll} \gg \nu_{site}$ is apparently valid, we can assume that $\nu_{tot} \approx \nu_{site}$ and

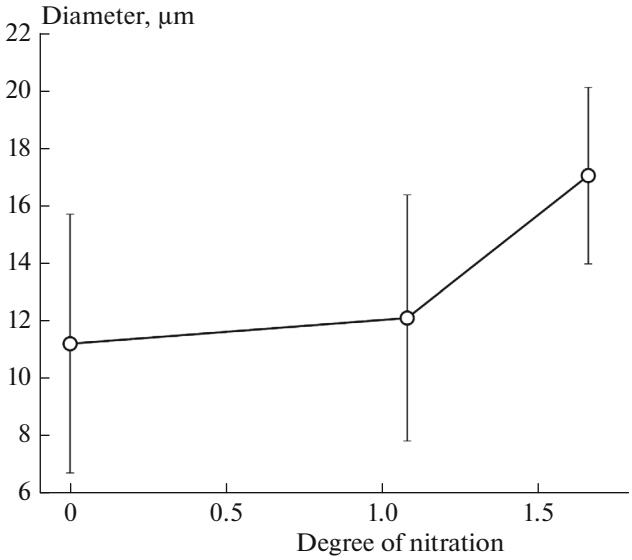

Fig. 8. Dependence of the average thickness of the cellulose/NC fiber on the nitrogen content according to electron microscopy. Large measurement errors are associated with the initial variability of the fiber thickness. Data on thickness are given for $\sim 10^2$ fibers.

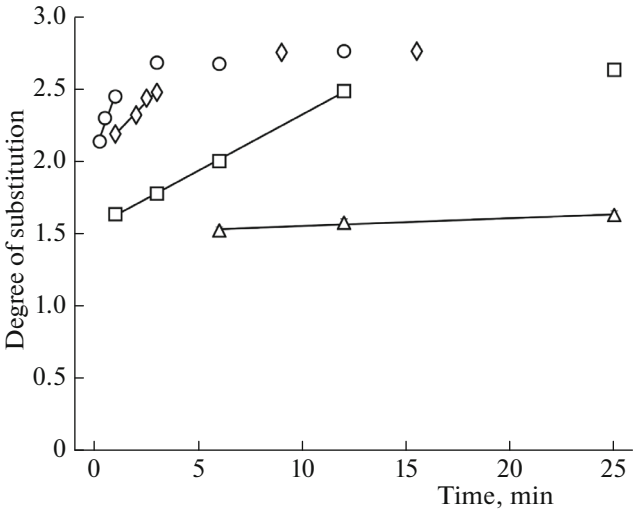

Fig. 9. Kinetic curves of nitration of wood cellulose at the different temperatures: triangle, −10°C; square, 2°C; diamond, 20°C, and circle, 34°C. The solid lines show the linear portions of the curves.

there is a significant entropy contribution responsible for the reaction rate because the formation of a reaction site is physically associated with fibril untwisting cooperative processes. According to the literature data, the nitration reaction is nearly activationless [24]; therefore, the activation energy value can be attributed to the energy of complementary intermolecular interaction of the glucopyranose rings of cellulose, which provides a close packing of the rings and

hinders the penetration of the nitrating agent into the crystalline regions.

A simple estimate of intermolecular interaction energy yields a similar value. Cellulose nanofibrils contain, on the average, two interchain hydrogen bonds per glucopyranose unit [1], which gives a binding energy of chains of about 30 kJ/mol. The helicity of cellulose microfibrils provides the complementarity of interaction of the cellulose chains. A glucose residue consists of 21 atoms; assuming that the average energy of the van der Waals interaction between two atoms is ~1 kJ/mol, for the interchain binding energy, we obtain a gain of ~20 kJ/mol. Thus, for the average binding energy of cellulose chains, we obtain a value of ~50 kJ/mol, which is close to the previously calculated activation energy of the nitration process (E_a).

At the same time, it is known that nitration is an exothermic reaction accompanied by a significant—about 130 kJ/mol—heat evolution [29]. Since the kinetic characteristics are markedly sensitive to changes in temperature by as little as 10°C, the local overheating in the exothermic reaction has a considerably smaller value. Otherwise, the reaction mixture temperature registered by external devices would be substantially lower than the actual temperature at which the reaction occurs and the temperature dependence would be much less pronounced. To explain this effect, it is necessary to estimate the size of the region in which the reaction occurs and the thermalization time. Thermalization time τ of the energy released in the exothermic reaction in the form of nonequilibrium phonons, particularly high-energy phonons, in the thermalization region of size R, is determined by the cooling of it to a thermostat temperature:

$$\tau = \frac{c\rho R^2}{\lambda}, \quad (5)$$

where c is the heat capacity, ρ is the density, and λ is the heat conductivity. For water, after substitution of respective values, at thermalization region size R of 1–10 nm, this estimate yields a value of $\tau \sim 10^{-11}$–10^{-9} s. In this case, R is an adjustable parameter, which is equal to the distance a high-energy phonon travels before it undergoes thermalization; it was estimated taking into account the crystallinity of the lattice of the elementary fibril. At the same time, during nitration, there occur no more than 10^{21} elementary events of nitration per cubic centimeter per second. In this case, in the attached volume of radius R of the glucopyranose ring ($V \sim 4 \times 10^{-18}$ cm^3), there occur no more than 4×10^3 substitution events per about second or one event per 2.5×10^{-4} s. Further, with allowance for the τ value, it becomes obvious that each successive event of nitration in the thermalization region occurs at the thermostat temperature. It is this feature that is responsible for the sensitivity of the kinetic parameters of the highly exothermic nitration reaction to small changes in the thermostat temperature.

AFM studies of the cellulose feedstocks revealed that the untwisting of the cellulose fibers occurs at the end faces, as evidenced by the formation of a dispersed phase observed in the fiber topography profile. Note that the observed untwisting is apparently geometrically similar to the untwisting of supercoiled microscopic supramolecular TFAAS strings (Fig. 10c). Let us sequentially consider the dependence of the nitrogen content on the different factors that reduce the binding of elementary fibrils and fibrils in a supercoiled state (in "bundles") using the example of the cellulose manufactured at the Syassky PPM. Thus, in the case of nitration of the unrefined cellulose, the degree of nitration achieves 11.46 ± 0.34%. After refining and the removal of low-molecular-weight cellulose fractions binding the fibrils, the nitrogen content increases to 12.10 ± 0.36%.

This process is also intensified with the appearance of charged groups on the lateral surface of the fibrils. For example, the appearance of sulfo groups on the surface of the cellulose fibers gives rise to a negative charge on it. In general, the mechanism of this reaction can be similar to the S_N1 mechanism of the lignin sulfonation reaction [1]. In an acid medium, a carbocation is formed; it can be subsequently attacked by the sulfite present in the medium:

$$R^+ + HSO_3^- \rightarrow R{-}O{-}SO_2H,$$

$$R{-}O{-}SO_2H + H_2O \rightarrow R{-}O{-}SO_2^- + H_3O^+.$$

The resulting sulfite is unstable and analytically undetectable; however, even a very small excess negative charge is sufficient for the untwisting process. Similar charges on individual cellulose chains in the composition of the elementary fibril lead to their repulsion; this process should intensify the untwisting. In fact, in a $NaHSO_3$ solution, the amplitude of CD spectra decreases in a wavelength region of 250 nm; this decrease apparently corresponds to the effective untwisting of the elementary fibrils of the NNC to macromolecules (Fig. 11). Since a strict interpretation of CD spectra is severely hindered, particularly for complex systems, such as a NNC gel, here, the interpretation of the observed chirooptic effect is also based on the assumption that the untwisting of supercoiled strings in the model TFAAS system is also accompanied by a similar decrease in the CD intensity in a similar wavelength range [14].

The available threshold effect consists in a variation in CD, rather than in the solution absorption in general. In fact, the threshold effect corresponds to a $NaHSO_3$ concentration in the final mixture of 2% (0.16 M); in addition, the measured absorption spectra in a range of 220–350 nm for NNC gel samples with the same $NaHSO_3$ concentrations showed good agreement for sub- and post-threshold concentrations (2.5%, 0.2 M).

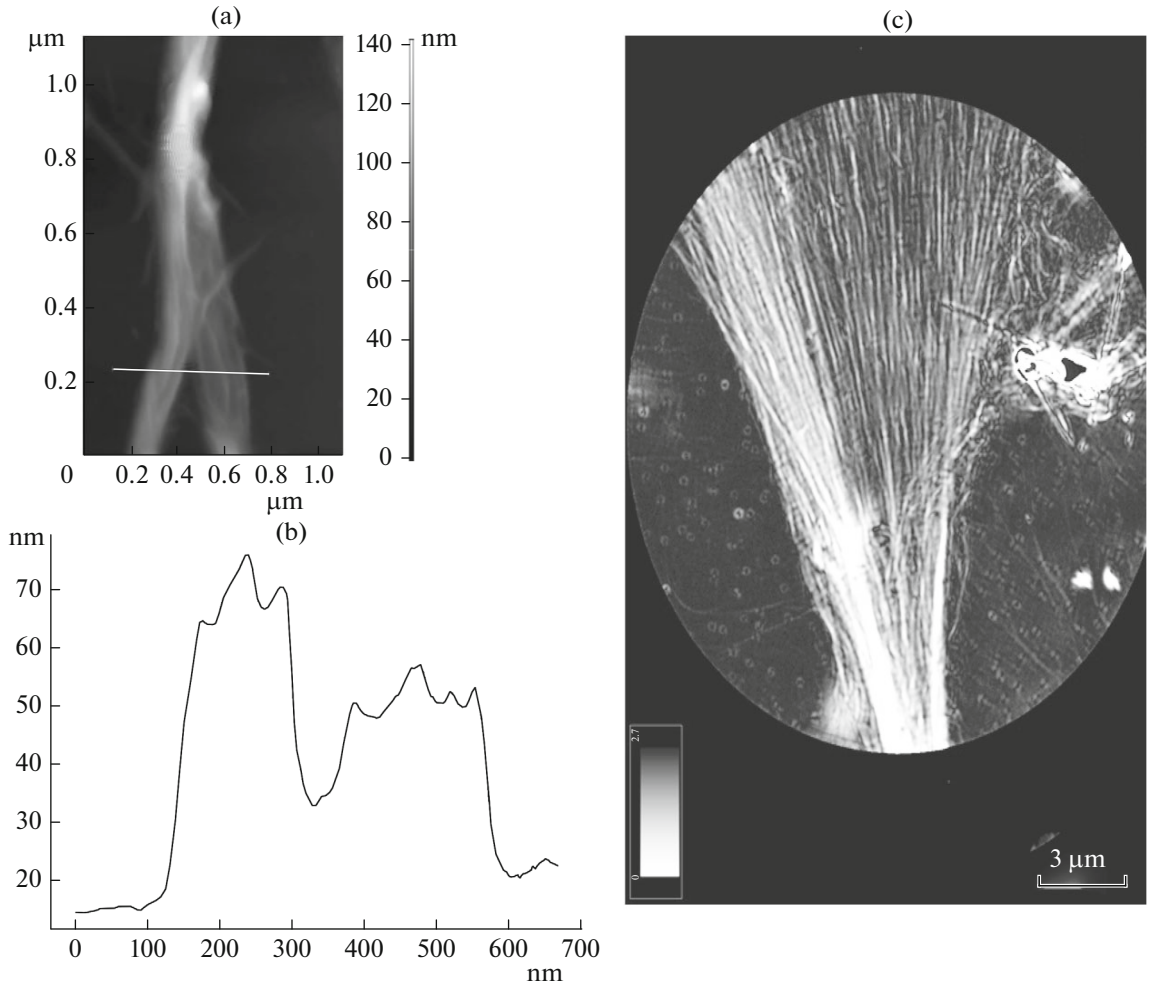

Fig. 10. Destruction (untwisting) of structures: (a) a topographic AFM image of a cellulose fiber with a marked region, (b) the surface profile of the marked region of the fiber, and (c) an optical micrograph showing the untwisting of a supramolecular TFAAS-5 string [11].

The treatment of the cellulose produced at the Syassky PPM (SKhZh) with a 1% $NaHSO_3$ solution at a temperature of 60°C for 200 min leads to an increase in the nitrogen content in the final nitration product to 12.7 ± 0.4% compared with the nitrogen content obtained in the nitration of the original cellulose 10.8 ± 0.3%. Experimental data on the nitration of the refined cellulose (SKhZh) also show that the treatment of the cellulose with 1% $NaHSO_3$ at a temperature of 60°C for 200 min leads to an increase in the degree of nitration from 12.1 ± 0.4% for the original refined cellulose to 12.9 ± 0.4% (Table 3).

Another way to reduce the strength of interaction of elementary fibrils is to provide a decrease in the van der Waals interaction of the fibrils. Thus, during the treatment of the refined cellulose (SKhZh) samples with acetone, the polar OH groups on the surface of the elementary fibrils are doped; that is, they attach acetone molecules via the formation of a strong hydrogen bond. Accordingly, the fraction of OH groups on the surface decreases, while the fraction of methyl groups with lower polarizability increases. The strength of the van der Waals interaction of the neighboring functional groups decreases because it is proportional to the product of polarizability of the groups. Therefore, the macroscopic van der Waals interaction of the fibrils should decrease, while the degree of nitration thereof should increase (Table 3).

Treatment with a 0.1 M H_3BO_3 solution at a temperature of 60°C for 200 min also leads to an increase in the degree of nitration to 13.07 ± 0.39 apparently owing to the plasticization of the cellulose matrix by H_3BO_3. Since the treatment with boric acid does not lead to significant changes in the CD spectra of cellulose gels, the observed effect is apparently attributed also to the weakening of the interaction of the cellulose macromolecules owing to the formation of a competing lattice of hydrogen bonds; it is this feature that facilitates untwisting during nitration.

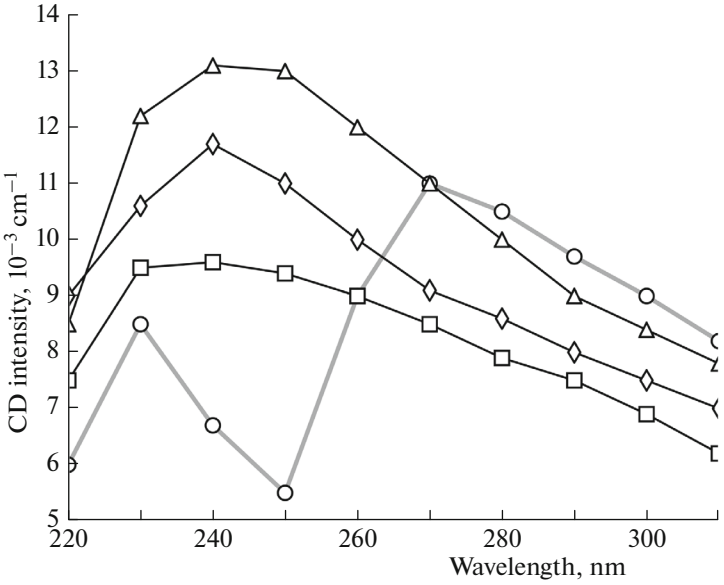

Fig. 11. CD spectra of cellulose at the different $NaHSO_3$ concentrations: triangle, 0.5%; diamond, 1%; square, 1.5%; and circle, 2%. A variation in the monotonic behavior of the CD dependence on sodium hydrosulfite concentration is clearly seen.

Consider differences in the rates of nitration of wood, flax, and cotton celluloses, which can easily be related to different diameters of the elementary cellulose fibrils characteristic of these plants [20]. The distance between the fibers in the contact areas is limited to the profile of the fibers. On the assumption of a geometric similarity between the hierarchical levels of the structural organization of cellulose, the scale of their profile will be proportional to the fiber diameter. Thus, effective distance h between the fibers in the contact areas is proportional to the diameter of these fibers. In view of the same similarity, pitch H of the helix formed via the interweaving of thinner fibers is also proportional to their diameter:

$$h = \varepsilon D, \quad \varepsilon \ll 1, \quad H = \alpha d, \quad \alpha \ll 1, \tag{6}$$

where ε and α are the respective proportionality coefficients.

The elastic energy due to the helimerization of fibers is calculated as follows. Let the fiber be an elastic helically curved rod. The curve of the fiber in the helical twist can be considered weak. Elastic energy W_{el} of the weakly curved rod is defined by the following relationship [30]:

$$W_{el} = \frac{E}{2}\int I_1\left(\frac{d^2Y}{dz^2}\right)^2 + I_2\left(\frac{d^2X}{dx^2}\right)^2 dz, \tag{7}$$

where E is the Young's modulus of the rod material; the z axis is directed along the axis of the undeformed rod; $X(z)$ and $Y(z)$ are the deviations of the rod axis from the z axis owing to deformation along the x and y axes, respectively; and I_1 and I_2 are the second moments of area relative to the x and y axes, respectively. In the case of a rod with a circular cross section, for the second moments of area, we obtain

$$I_1 = I_2 = \frac{\pi d^4}{64}. \tag{8}$$

To describe the helical deformation of the rod, the following expressions are taken for a uniform twist of the rod with pitch H and amplitude A:

$$X(z) = A\cos\frac{z}{H}, \quad Y(z) = A\sin\frac{z}{H}. \tag{9}$$

Hence,

$$\frac{d^2X}{dz^2} = -\left(\frac{A}{H^2}\right)\cos\frac{z}{H}, \quad \frac{d^2Y}{dz^2} = -\left(\frac{A}{H^2}\right)\sin\frac{z}{H}. \tag{10}$$

From Eqs. (8) and (10), we find

$$I_1\left(\frac{d^2Y}{dz^2}\right)^2 + I_2\left(\frac{d^2X}{dx^2}\right)^2 = \frac{\pi d^4 A}{64H^4}, \tag{11}$$

that is, the integrand in Eq. (7) is independent of z; therefore, the integration over z is reduced to multiplying it by the fiber length. Take into account that elastic energy is exhibited by both of the interwoven fibers. Thus, their total elastic energy per unit length W_{el} will be as follows:

$$W_{el} = \frac{\pi E d^4 A^2}{64H^4}. \tag{12}$$

Twist amplitude A (measured from the deviation from the initial position of the geometric center of the rod with a circular cross section) can easily be expressed in terms of fiber diameter d and distance h between the fibers:

$$A = d + h. \quad (13)$$

For distance h between the fibers and helix pitch H, Eq. (6) can be used. Eventually, taking into account that $\varepsilon \ll 1$, Eq. (12) for the specific (per unit length) elastic energy of the interwoven fibers takes the form

Global: $\varepsilon \ll 1$ is incorrect.

$$W_{el} = \left[\frac{\pi(1+\varepsilon)^2}{64\alpha^4}\right] Ed^2 \sim \frac{\pi}{64\alpha^4} Ed^2. \quad (14)$$

Thus, in terms of the model under discussion, the elastic energy of interwoven fibers (per unit length) is directly proportional to the square of the fiber diameter; that is, the thinner (wood) fibers undergo repulsion (owing to a tendency to straighten themselves) weaker than the thicker (cotton) fibers do. Experimental value of α is ~10^2; that is, the helix pitch of the fiber is on the order of a hundred of the fiber diameters. However, even in the case of a high Young's modulus of ~10^{11} N/m^2, which is characteristic of the hardest crystals, from Eq. (14) in a diameter range of d = 3–7 nm, we obtain $W_{el} = 2 \times 10^{-6}$–$10^{-5}$ eV/nm, which is 4–5 orders of magnitude lower than the energy of the van der Waals attraction of fibers given in Table 4. Thus, in the case of a supercoiled packing of the fiber with this pitch, the elastic energy is negligible and will not be considered in further calculations.

Owing to the partial sulfonation of cellulose fibers subjected to treatment with a sodium hydrosulfite solution, similar (negative) elementary charges e appear on the surface of thin fibers and lead to the repulsion of the fibers. Electrostatic repulsion is hindered by van der Waals attraction. Elementary fibrils twisted into a helix with a large pitch can be represented as parallel at a length longer than L at which the helix portion weakly deviates. In this case, van der Waals attraction energy W_{vdW} of the fibers in a portion with length L is as follows [14]:

$$W_{vdW} = -\frac{AL}{24}\left(\frac{d}{2h^3}\right)^{1/2}. \quad (15)$$

The van der Waals attraction force is determined by differentiation with respect to h:

$$F_{vdW} = -\frac{AL}{16}\left(\frac{d}{2h^5}\right)^{1/2}. \quad (16)$$

The van der Waals force per unit length of the attracted fibers will be as follows:

$$f_{vdW} = \frac{AL}{16}\left(\frac{d}{2h^5}\right)^{1/2} = \frac{A}{16d^2}(2\varepsilon^5)^{1/2} \sim \frac{1}{d^2}. \quad (17)$$

Coulomb repulsion force F_Q, which provides the repulsion and untwisting of fibers, can be regarded as a mutual repulsion of two similarly charged plates with surface charge density σ, length L, and width $l = \nu d$, where $\nu \sim 0.1$ is the proportionality coefficient. This force is as follows:

Table 3. Nitrogen content in NC prepared by physicochemical modification of cellulose

Sample designation	Nitrogen content, wt %
SZhP nontreated	10.8 ± 0.3
SZhP, 1% $NaHSO_3$ solution, 60°C, 200 min	12.67 ± 0.38
SKhP (α)	12.1 ± 0.4
SKhZh (α), 1% $NaHSO_3$ solution, 60°C, 200 min	12.9 ± 0.4
SKhZh (α), acetone (soaking)	12.96 ± 0.39
SKhZh (α), 0.1 M H_3BO_3, 60°C, 200 min	13.07 ± 0.39
AKhZh (α)	13.46 ± 0.40
VLV nontreated	11.28 ± 0.37
VLV (α)	13.17 ± 0.39

Table 4. Energy (eV/nm) of van der Waals attraction and electrostatic repulsion of cellulose nanofibrils with different diameters

d, nm	W_{vdW}	W_{el}	$W = W_{vdW} - W_{el}$
3	0.185	0.013	0.172
4	0.139	0.022	0.117
5	0.111	0.036	0.075
6	0.092	0.051	0.041
7	0.079	0.070	0.009

$$F_Q = \frac{2\pi\sigma lL}{\xi}, \quad (18)$$

where ξ is the dielectric permeability of the medium. The Coulomb force per unit length of the fibers will be

$$f_Q = \frac{2\pi\sigma^2 I}{\xi} = \frac{2\pi\sigma^2 \nu d}{\xi} \sim d. \quad (19)$$

The threshold linear concentration of elementary charges along the fiber at which the forces of mutual attraction and repulsion become equal will be as follows:

$$n_L = \left[\frac{A\varepsilon\nu}{32(2\xi^5)^{1/2}\pi e^2 d}\right]^{1/2}. \quad (20)$$

Expressions (17) and (19) suggest the following:

—In the case of thinner fibers of wood cellulose, the Coulomb force normalized per unit length that provides the untwisting of the fibers is lower than the force for thicker fibers of cotton and flax celluloses because the force is proportional to the fiber diameter.

—In the case of thinner fibers of wood cellulose, the van der Waals attractive force of fibers normalized per unit length that provides the winding of the fibers is higher than the force for thicker fibers of cotton cel-

Table 5. Range of location of charged groups on cellulose nanofibrils that is sufficient for the untwisting of the respective microfibrils as a function of nanofibril thickness

d, nm	L_{min}, nm	L_{max}, nm
3	1.3	26.7
4	1.5	29.5
5	1.8	36.8
6	2.8	56.1
7	11.0	219.0

Table 6. Energy of van der Waals attraction and linear charge density compensating for it as a function of the linear charge density versus the fibril diameter

d, nm	W_{vdW}, eV/nm	n_L
3	0.185	0.23
4	0.139	0.20
5	0.111	0.18
6	0.092	0.16
7	0.079	0.15
8	0.069	0.14
9	0.062	0.13

lulose because the force is inversely proportional to the square of the diameter. The respective van der Waals attraction energy values and the linear densities of the charge sufficient for compensating for it are listed in Tables 5 and 6.

Thus, in the presence of a fluctuating charge of the same magnitude, cotton cellulose fibers must undergo more effective untwisting under the action of repulsing Coulomb forces. Apparently, this feature is another factor leading to a higher degree of nitration of this cellulose compared with that of wood and flax celluloses.

CONCLUSIONS

The kinetics of cellulose nitration has been studied; it has been revealed that it is of zero order in the fast reaction stage. It has been found that the activation energy of the reaction is $E_a \sim 46$ kJ/mol and the preexponential factor of the rate constant is $K_0 \sim 10^5$ s^{-1}.

It has been theoretically shown that the nitration process is limited to the macroscopic dynamics of untwisting of cellulose fibers and fibrils, elementary fibrils, and macromolecules, rather than to the diffusion of the reactants. This assumption has been experimentally confirmed by the zero order of the kinetics of nitration, the preexponential factor K_0 and activation energy E_a values, AFM micrographs, optical microscopy data, a decrease in the amplitude of the CD spectra of cellulose in $NaHSO_3$ solutions, and a large body of data on nitration of the samples (Table 3).

In terms of physics, this finding is attributed to the formation of a Born potential barrier of ~1 eV to the penetration of the nitronium ion into the internal volume of nanofibrils with completely nitrated (hydrophobic) outer layers at a degree of substitution of ~1.3. This barrier arises because of spatial restrictions in the molecular dynamics of the macromolecules and a free-volume deficit associated with the supercoiling of the elementary cellulose fibrils. Phenomenologically, this feature corresponds to the impossibility of transition of the ion from the RAM with a dielectric permeability of $\varepsilon \sim 100$ into the nitrated regions of the nanofibrils with $\varepsilon \sim 3$–5 across a barrier of ~1 eV.

A phenomenological model to describe the electrostatic and van der Waals interactions of elementary fibrils has been constructed on the basis of similarity of scales in the system of supercoiled elementary fibrils. According to this model, during nitration, the free-volume deficit is compensated for by the Coulomb repulsion of similarly charged elementary fibrils attracted by van der Waals forces and the subsequent untwisting of the fibrils.

This process occurs more effectively in cotton fibers; this fact is attributed to the large diameter of their elementary fibrils, which have a thickness of about 7–9 nm. In thin fibrils of wood cellulose strongly bound by low-molecular-weight celluloses (3–5 nm), the process is intensified during cellulose refining (Table 3). In weakly bound cotton fibers, the untwisting of thicker elementary fibrils (7–9 nm) can occur spontaneously because of the fluctuating surface charge that provides repulsion and untwisting of the fibrils; this feature leads to a higher nitrogen content after the nitration of cotton cellulose. In the intermediate case of flax fibers containing elementary fibrils with a diameter of 5–6 nm, it is also necessary to remove low-molecular-weight celluloses; however, their fraction is most probably lower because a fairly effective nitration process can occur without refining (Table 3).

It has been experimentally shown that there are three alternative paths to select an optimum technological mode. The first path is to reduce the amount of the "glue" binding nanofibrils via removing lignin and amorphous low-molecular-weight celluloses during refining. Next, it is possible to increase the specific surface charge of nanofibrils, for example, by a treatment with sulfurous acid. Finally, the energy of the van der Waals attraction between the elementary fibrils can be decreased, for example, by a pretreatment with acetone or boric acid.

Thus, the effect of the helical structural and dynamic factors on the occurrence of the cellulose nitration reaction has been studied for the first time; it has been found that the chemical reaction includes a set of physical stages that are responsible for the reac-

tion rate. The proposed physical mechanism of decrease in the cellulose nitration rate explains the entire range of effect observed during the nitration of raw materials of different origin.

REFERENCES

1. N. I. Nikitin, *Chemistry of Wood and Cellulose* (Akad. Nauk SSSR, Moscow, Leningrad, 1962) [in Russian].
2. I. L. Knunyants and N. S. Zefirov, *Chemical Encyclopedy* (Sov. Entsiklopediya, Moscow, 1988) [in Russian].
3. E. M. Belova, N. G. Vais, V. F. Sopin, A. I. Kazakov, Yu. I. Rubtsov, G. B. Manelis, and G. N. Marchenko, Russ. Chem. Bull. **38**, 2244 (1989).
4. V. A. Rafeev, Yu. L. Rubtsov, T. V. Sorokina, and N. V. Chukanov, Russ. Chem. Bull. **48**, 66 (1999).
5. V. I. Kovalenko, V. F. Sopin, and G. M. Khrapkovskii, *Structural Kinetic Features of Preparation and Thermal Degradation of Cellulose Nitrate* (Nauka, Moscow, 2005) [in Russian].
6. G. N. Marchenko, V. F. Sopin, et al., Vysokomol. Soedin., No. 5, 1066 (1989).
7. V. A. Rafeev, Yu. L. Rubtsov, and T. V. Sorokina, Russ. Chem. Bull. **45**, 328 (1996).
8. V. A. Rafeev, Yu. L. Rubtsov, and T. V. Sorokina, Russ. Chem. Bull. **45**, 1879 (1996).
9. A. I. Mikhailov, L. P. Bel'kova, and V. S. Gromov, Khim. Drev., No. 6, 50 (1980).
10. A. I. Mikhailov, L. P. Bel'kova, and V. S. Gromov, Khim. Drev., No. 6, 59 (1980).
11. E. T. Denisov, O. M. Sarkisov, and G. I. Likhtenshtein, *Chemical Kinetics* (Khimiya, Moscow, 2000) [in Russian].
12. S. V. Stovbun, A. A. Skoblin, A. M. Zanin, et al., Bull. Exp. Biol. Med. **154**, 34 (2012).
13. V. A. Tverdislov, Biophysics **58**, 128 (2013).
14. S. V. Stovbun and A. A. Skoblin, Mosc. Univ. Phys. Bull. **67**, 317 (2012).
15. D. V. Zlenko and S. V. Stovbun, Russ. J. Phys. Chem. B **8**, 499 (2014).
16. F. Revol, H. Bradford, J. Giasson, R. H. Marchessault, and D. G. Gray, Int. J. Biol. Macromol. **14**, 170 (1992).
17. G. C. Ruben, G. H. Bokelman, and W. Krakow, Plant Cell Wall **399**, 78 (1989).
18. K. Muhlethaler, Ann. Rev. Plant Phys. **42** (18), 24 (1967).
19. A. N. J. Heyn, J. Cell Biol. **9**, 181 (1966).
20. R. H. Newman, Solid State Nucl. Magn. Reson., 15 (1999).
21. A. N. Fernandes, L. H. Thomasb, C. M. Altanerc, et al., Proc. Natl. Acad. Sci. **108**, E1195 (2011).
22. C. Somerville, Ann. Rev. Cell Dev. Biol. **22**, 53 (2006).
23. G. Murch, Diffusion in Crystalline Solids, N.Y., Acad. Press, 1984.
24. C. K. Ingold, *Structure and Mechanism in Organic Chemistry* (Cornell Univ., Ithaca, 1969).
25. V. I. Gol'danskii, L. I. Trakhtenberg, and V. N. Flerov, *Tunneling Phenomena in Chemical Physics* (Nauka, Moscow, 1986) [in Russian].
26. J. N. Israelachvili, *Intermolecular and Surface Forces* (Academic, New York, 2007).
27. E. V. Novozhilov, D. G. Chukhchin, K. Yu. Terent'ev, and I. A. Khadyko, Khim. Rastit. Syr'ya, No. 2, 15 (2012).
28. A. A. Silin, *Friction and We* (Nauka, Moscow, 1987) [in Russian].
29. G. Considine, *Van Norstrand's Scientific Encyclopedia* (Wiley, New York, 2006).
30. L. D. Landau and E. M. Lifshitz, *Course of Theoretical Physics,* Vol. 7: *Theory of Elasticity* (Nauka, Moscow, 1987; Pergamon Press, New York, 1986).

Translated by M. Timoshinina